Engineering Fracture Mechanics 150 (2015) 135–142

Contents lists available at ScienceDirect

Engineering Fracture Mechanics

journal homepage: www.elsevier.com/locate/engfracmech

Size-dependent brittle-to-ductile transition in GaAs nano-rods

J. Wang [a,b], Y.G. Shen [b], F. Song [a], F.J. Ke [c], Y.L. Bai [a], C. Lu [d,*]

[a] State Key Laboratory of Nonlinear Mechanics (LNM), Institute of Mechanics, Chinese Academy of Sciences, Beijing 100190, China
[b] Department of Mechanical and Biomedical Engineering, City University of Hong Kong, Kowloon, Hong Kong, China
[c] School of Physics and Nuclear Energy Engineering, Beihang University, Beijing 100191, China
[d] Department of Mechanical Engineering, Curtin University, Perth, WA 6845, Australia

ARTICLE INFO

Article history:
Received 3 December 2014
Received in revised form 10 March 2015
Accepted 7 April 2015
Available online 16 April 2015

Keywords:
Molecular dynamics simulation
GaAs nano-rods
Brittle-to-ductile transition
Dislocation
Size effect

ABSTRACT

GaAs is brittle at room temperature at the macro-scale; however, ductility emerges when its characteristic dimension reduces to the nano-scale. Using molecular dynamics simulations, we reveal that there is a brittle-to-ductile transition in GaAs nano-rods due to the competition between generation of cracks and initiation of dislocations. Such a competition is sensitive to aspect ratios of nano-rods. These results well explain experimentally observed ductility of GaAs nano-rods and have important implications for the design of semiconductor materials with tailored mechanical properties.

1. Introduction

Binary compound semiconductor nano-wires and nano-rods (NRs), such as GaAs, ZnO and SiC, are attractive materials due to their remarkable physical, electrical, and mechanical properties. These materials have many potential industrial and engineering applications, including nano-building blocks in nano-electronic components and optoelectronic and electromechanical devices in micro-electro-mechanical systems [1–4]. For instance, GaAs possesses direct band gaps and high electron mobility. Thus, GaAs has many advantages over elemental semiconductors like silicon and its applications range from efficient photovoltaic devices to radio-frequency electronics and optoelectronics [1]. Mechanical and electrical properties of materials at nano-scales, as is well known, are significantly different from their coarse-grained counterparts [5–7]. The giant piezoelectric size effect and size-dependent Young's modulus are identified in ZnO nano-wires [8–11]. Moreover, the large plastic deformation can be induced in SiC nano-wires at room temperature [12–14]. Recently, the nano-size effect on mechanical properties of semiconductors has been a hot topic in nanotechnology and nanoscience [15–17]. However, the mechanical properties of GaAs NRs remain largely unexplored due to the lack of efficient synthetic methods [18].

By using Au nanoparticle-catalyzed metalorganic chemical vapor deposition, vertically aligned epitaxial zinc-blende (ZB) structured GaAs NRs with an excellent crystallographic quality and an optimal shape have successfully been grown [18]. The wide lateral dimensions of as-synthesized GaAs NRs, ranging from ~9 to 160 nm, provide a possibility to examine the size effect of their mechanical properties. Based on the *in situ* nano-indentation and tensile straining transmission electron microscopy technique, it is shown that the lateral dimension has a significant influence on the mechanical behavior of

* Corresponding author. Tel.: +61 8 92664562; fax: +61 8 92662681.
E-mail address: C.Lu@curtin.edu.au (C. Lu).

http://dx.doi.org/10.1016/j.engfracmech.2015.04.006
0013-7944/

Nomenclature

Latin characters

A/W	potential parameters of the pairwise interaction
$B/C/l$	potential parameters of the three-body interaction
e	the elementary electron charge
h	length of a nano-rod
I	the moment of inertia
R	interatomic distance
S	the cross sectional area of a nano-rod
V	interatomic interaction
Z	the effective atomic charge

Greek characters

α	the coefficient of the screened Coulomb interaction
ε	strain
η	the exponent of the steric repulsion
θ	the angle between bonds
Θ	step function
σ	ionic radii

Sub/superscripts

$\bullet_c$	related to the cutoff length of pairwise interaction
$\bullet^{\mathrm{cr}}$	related to the critical properties of buckling
$\bullet_{\mathrm{Euler}}$	related to the conventional Euler buckling model
$\bullet_{ijk}$	related to atoms i, j and k
$\bullet_0$	related to the cutoff length of three-body interaction
$\bullet_{1s}$, $\bullet_{4s}$	related to the screen length of the Coulomb interaction
$\bullet^{(2)}$, $\bullet^{(3)}$	related to the pairwise and three-body interactions, respectively

Abbreviations

AR	aspect ratio
FCC	face-centered cubic
MD	molecular dynamics
NR	nano-rod
ZB	zinc-blende

GaAs NRs. Specifically, NRs with a lateral dimension less than 12 nm exhibit a repeatable self-healing ability due to the near-field electrostatic interaction [19,20]. It is also found that Young's modulus of GaAs NRs decreases as the increase of their lateral dimensions because of a core–shell structure and a higher stress state on the surface area [21]. Most importantly, the compressive plastic deformation is recognized in GaAs NRs with a lateral dimension of less than 25 nm, whereas GaAs NRs with a larger lateral dimension only show brittle fracture [21]. It is expected that there is a size-dependent brittle-to-ductile transition in GaAs NRs. However, the physical mechanism and nanostructure-deformation relationships behind these exceptional mechanical properties remain elusive due to limitations in current experimental devices and techniques.

To identify the critical size that leads to a brittle-to-ductile transition in GaAs NRs, it is instructive to recall extant experimental protocols of *in-situ* compressive tests [21–24]. For quantitatively testing the mechanical properties of GaAs NRs, a substrate consisting of NRs was mounted on a Hysitron PicoIndenter holder (PI 95) inside a JEOL JEM-2100 transmission electron microscope. A NR was compressed along its axis by the PicoIndenter with a flat diamond punch. Such a displacement-controlled mode ran at a rate of 20 nm/s and its force and spatial resolutions are 0.3 μN and 1 nm, respectively [21]. The deformation process was recorded by transmission electron microscopy images and a real-time video at the speed of 30 frames per second [21,22]. In the compressive tests, there are two long-standing difficulties. On one hand, the force resolution (0.3 μN) is inadequate as the lateral dimension of a NR is below 55 nm and thus its mechanical properties cannot be obtained [21]. On the other hand, the structural evolution that induces to ductile deformation might escape from experimental observations since its speed ($\sim 10^3$ m/s in solids) is far more than that of a real-time video. Fortunately, atomistic simulations can be used to trace back these missing details.

This paper aims to investigate the compressive deformation of GaAs NRs by using molecular dynamics (MD) simulations that are introduced in Section 2. A size-dependent brittle-to-ductile transition is reported in Section 3 and its relevant mechanisms are discussed in Section 4. Finally, a summary is given in Section 5.

2. Molecular dynamics simulations

The ZB GaAs adopts an ordered sequence of three basic modules of tetrahedral bonding denoting as A, B and C (see Fig. 1a), where each module, consisting of a Ga–As pair, is a close packed plane. An as-synthesized GaAs NR has a threefold symmetry around the [1 1 1] axis with six (1 1 0) side facets [25]. Fig. 1b shows a typical computational model generated by the visual MD [26], with a cross-sectional dimension of 5.5 nm and an aspect ratio (AR) of 6:1. Free and periodic boundary conditions are implemented along the lateral and axial directions, respectively, to ensure the traction-free condition of a NR. To study the size effect, the lateral dimensions of NRs are chosen from 1.8 to 20 nm with the ARs varying from 4:1 to 24:1.

2.1. Interatomic interaction

A potential function with the form of

$$V = \sum_{i<j} V_{ij}^{(2)}(r_{ij}) + \sum_{i,j<k} V_{jik}^{(3)}(r_{ij}, r_{ik}) \tag{1}$$

is employed to the model with the two-body (Ga–Ga, Ga–As and As–As) and three-body covalent (Ga–As–Ga and As–Ga–As) interactions in GaAs, where r_{ij} is the distance between atoms i and j [27]. The two-body part can be written as

$$V_{ij}^{(2)}(r_{ij}) = A_{ij}\left(\frac{\sigma_i+\sigma_j}{r_{ij}}\right)^{\eta_{ij}} + \frac{Z_i Z_j}{r_{ij}}\exp(-r_{ij}/r_{1s}) - \frac{\alpha_i Z_j^2 \alpha_j Z_i^2}{2r_{ij}^4}\exp(-r_{ij}/r_{4s}) - \frac{W_{ij}}{r_{ij}^6}. \tag{2}$$

Here, the first term indicates the steric repulsion, defined by the strength prefactors A_{ij}, ionic radii σ_i and σ_j, and the exponent of steric repulsion η_{ij}. The second term is the screened Coulomb interaction due to the charge transfer with effective atomic charges (Z_i and Z_j) and a screen length of r_{1s} = 0.5 nm [27]. The third term corresponds to the charge dipole interaction due to large polarizability of negative ions, where r_{4s} = 0.375 nm is a screen length [27]. The last term is the induced dipole–dipole interaction with the van der Waals strength W_{ij}.

The three-body term in Eq. (1) combines the spatial and angular dependence in the form of

$$V_{jik}^{(3)}(r_{ij}, r_{ik}) = B_{jik}\exp\left(\frac{l}{r_{ij}-r_0}+\frac{l}{r_{ik}-r_0}\right)\times\frac{(\cos\theta_{jik}-\cos\bar{\theta}_{jik})^2}{1+C_{jik}(\cos\theta_{jik}-\cos\bar{\theta}_{jik})^2}\times\Theta(r_0-r_{ij})\Theta(r_0-r_{ik}), \tag{3}$$

where $B_{jik} = 7.9\times10^{-19}$ J is the strength of interaction, θ_{jik} is the angle between r_{ij} and r_{ik}, and C_{jik} = 20 and $\bar{\theta}_{jik}$ = 109.47° are constants. $\Theta(r_0 - r_{ij})$ is a step function. The characteristic length l and the three-body cutoff length r_0 are set to be 0.1 and 0.38 nm, respectively [27]. The two-body interaction is truncated at r_c = 0.75 nm [27]. To keep the potential and its first derivative continuous at r_c, the two-body interaction is shifted with

$$V_{(ij)}^{(2\ \text{shifted})}(r) = \begin{cases} V_{ij}^{(2)}(r) - V_{ij}^{(2)}(r_c) - (r-r_c)(dV_{ij}^{(2)}(r)/dr)_{r=r_c} & r \le r_c \\ 0 & r > r_c \end{cases}. \tag{4}$$

Parameters of the two-body potential are listed in Table 1 [27].

To simulate compressive loading, a deformation decrement along the [1 1 1] orientation is applied in two steps. First, an isothermal-isobaric ensemble is used to shorten a GaAs NR with a strain rate of -1×10^{-3} ps^{-1} for 1 ps [28]. This step

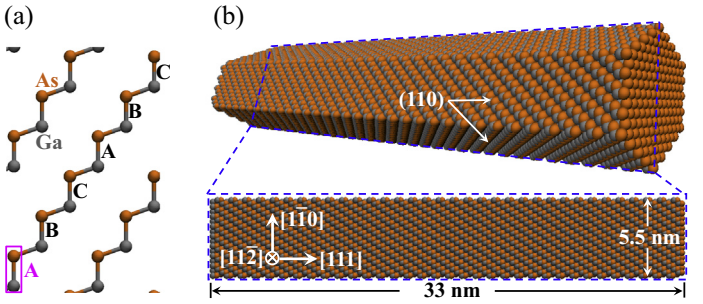

Fig. 1. Patterns of a ZB structured GaAs NR. (a) Three basic modules of tetrahedral bonding denoting as A, B and C, with each one consisting of a Ga–As pair marked by a box. (b) A sketch of a GaAs NR with an AR = 6:1.

Table 1
Two-body potential parameters used in the interaction potential of GaAs NRs [27]; see Eqs. 1–4. Here e represents the unit of electronic charge.

Atom type	σ (nm)	α (nm^3)	Z_i (e)	A_{ij} (10^{-19} J)	η_{ij}	W_{ij} (10^{-24} J nm^6)
Ga	0.095	0	0.9418			
As	0.1498	0.002	−0.9418			
Ga–Ga				16.4984	7	0
Ga–As				2.0623	9	58.916
As–As				2.0623	7	0

introduces a nominal strain of −0.1%. Second, the NR is relaxed for 6 ps with the axial strain being fixed via a canonical ensemble [29]. Before a compression load is applied, the sample is relaxed for 20 ps to obtain its stress-free state. The stress tensor is calculated by the classical virial formula and the system temperature is controlled at 300 K by the Nosé Hoover thermostat [30,31]. All simulations are carried out by using a modified version of the DL_POLY package, which can also be applied to predict ferroelectric behaviors of barium titanate [29,32].

2.2. Validation of the interatomic potential

It has been revealed that both surface elasticity and residual surface stress significantly affect the buckling behavior of nanowires under uniaxial compression [33,34]. A positive value of either surface elastic modulus or residual surface stress enhances the critical axial load and vice versa [34]. In GaAs NRs, there is a higher stress state on the surface area that causes the varying Young's modulus with their lateral dimensions [21]. This phenomenon can be described by the employed interatomic potential. The size-dependent Young's modulus is consistent with that observed in recent *in-situ* compressive tests of GaAs NRs [35]. Surface properties of GaAs for the (1 0 0), (1 1 0) and (1 1 1) surfaces predicted by the interatomic potential are also in agreement with *ab initio* calculations and experimental measurements such as the (1 0 0) surface reconstruction [27]. Thus, these factors, especially dimensions and surfaces, are of significance for us to reveal the brittle-to-ductile transition in GaAs NRs.

3. Results

3.1. Tensile brittleness and compressive ductility

Before compressive tests, tensile deformation of NRs is studied for comparison. It is observed that all samples exhibit the elastic stretch and subject to brittle fracture beyond the elastic limit. A NR with a lateral dimension of 5.5 nm and an AR = 6:1, as seen in the inset of Fig. 2a, encounters brittle fracture through breaking Ga–As bonds along neighboring (1 1 1) planes at a strain of 8.8%. Under compressive loading, however, it undergoes plastic deformation without failure even as strain reaches 20%. The relevant stress–strain curve shows a serrate feature with each precipitous stress drop (points A–C in Fig. 2a) corresponding to a dislocation event. Based on structural analysis, buckling that occurs beyond the elastic limit (see Fig. 2b) results in tensile stress on one side of the NR, while the opposite side is under a more severe compressive status. Two dislocations are detected to initiate on the surfaces of compressive sides and propagate along the $(1\ 1\ \bar{1})$ planes. In addition, these two dislocations cut through the surface of the sample as strain reaches 5.7%. Here, strain is simply defined as a reducing ratio of the distance between the two ends of a NR. As shown in Fig. 2c, with the increase of ARs, the critical

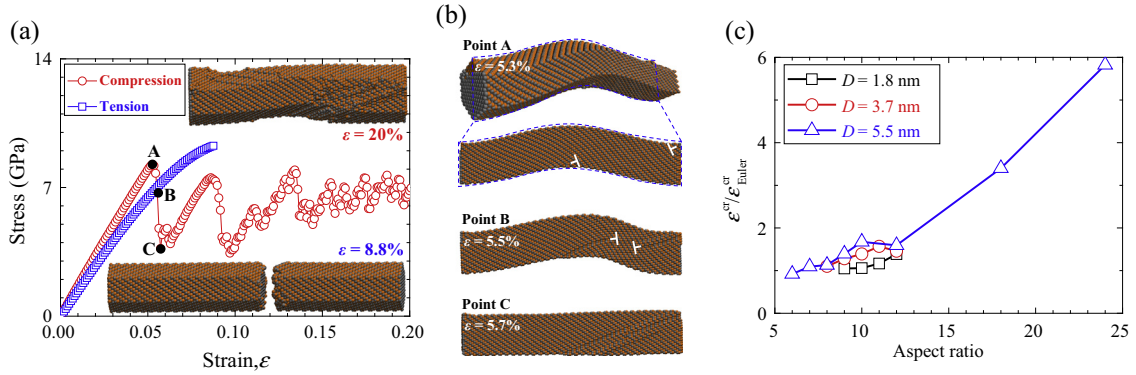

Fig. 2. Tensile brittleness and compressive ductility of a GaAs NR with a lateral dimension of 5.5 nm and an AR = 6:1. (a) Compressive and tensile stress–strain curves. (b) Dislocations initiate at compressive sides and propagate along the $(1\ 1\ \bar{1})$ planes. (c) The critical strain of axial buckling with respect to AR, where D represents the lateral dimension of a NR.

buckling strain ε^{cr} deviates from the critical Euler buckling strain ε^{cr}_{Euler}. Here, $\varepsilon^{cr}_{Euler} = 4\pi^2 I/(Sh^2)$, where I is the moment of inertia and S and h are the cross sectional area and length of a NR, respectively [33]. For a GaAs NR with a hexagonal lateral shape, $\varepsilon^{cr}_{Euler} = \frac{5\pi^2}{24}/(AR)^2$.

To measure Burgers vectors of dislocations in the case of compressive deformation of GaAs NRs, atomic trajectories are compared before and after slip events. Two types of partial dislocations, $1/6[\bar{1}\ 0\ \bar{1}]$ and $1/6[1\ 1\ \bar{2}]$, are identified. Fig. 3a sketches slip orientations of the two dislocations on the $(1\ 1\ \bar{1})$ plane. Fig. 3b and c demonstrate that, to propagate these dislocations, Ga–As bonds on the intra-close packed planes have to be broken and re-bonded. Fig. 3d shows a snapshot after the two dislocations penetrate though the surface of a sample.

3.2. Length-dependent brittle-to-ductile transition

The compressive behavior of GaAs NRs significantly depends on their ARs. Taking the sample with a lateral dimension of 5.5 nm as an example, an unambiguous ductile to brittle transition is detected at the critical AR of 9:1. Fig. 4a shows stress–strain curves of samples with various ARs. It is seen that strain at the elastic limit reduces by 34% from 5.3% to 3.5% as the AR increases from 6:1 to 9:1. Moreover, the NRs with AR = 6:1 and 7:1 generate plastic deformation with compressive strain more than 20% due to multiple dislocation activities. However, as the AR further increases to 8:1, brittle fracture happens as strain reaches 10.3% although dislocation activities lead to plastic deformation after the elastic limit (see Fig. 4b). It is of interest to note that, as the AR exceeds 9:1, brittle fracture occurs due to the generation of cracks. It is also worth noting that such a crack initiates at the tensile side via breaking Ga–As bonds along the neighboring (1 1 1) planes. The crack transversely expands and eventually results in brittle fracture of the sample.

3.3. Effect of lateral dimensions

The critical AR for a brittle-to-ductile transition in GaAs NRs is size-dependent. Fig. 5a is snapshots of three GaAs NRs with the same lateral dimension of 15 nm and different ARs: 4:1, 5:1 and 6:1, respectively. In the first case, a dislocation cuts through the sample. Such a deformation is referred to as the ductile behavior. The second one is referred to as the semi-brittle behavior, where a dislocation initiates before a crack. However, brittle fracture occurs before any dislocation traverses the sample. The last case is brittle because prior to initiation of a dislocation, a crack appears (see Fig. 5a), where dislocation lines and crack surface are visualized by using the dislocation extracting algorithm [36]. The size-dependent deformation behavior, as summarized in Fig. 5b, can be used to specify the critical size for distinguishing between brittle and ductile behaviors in GaAs NRs.

4. Discussion

Tensile and compressive tests have shown that GaAs NRs under tensile loading terminate with brittle fracture while ductile behavior only appears in the case of compressive deformation via dislocation activities. Similar phenomenon is also observed in binary compound semiconductor (ZB SiC) nano-wires [12–14,37]. During tension, a GaAs NR deforms uniformly along its axis. It ultimately subjects to brittle fracture at the elastic limit. The brittle fracture stems from the break of Ga–As bonds along the neighboring (1 1 1) planes and thus smooth fracture surfaces are observed (see inset of Fig. 2a). However, in a

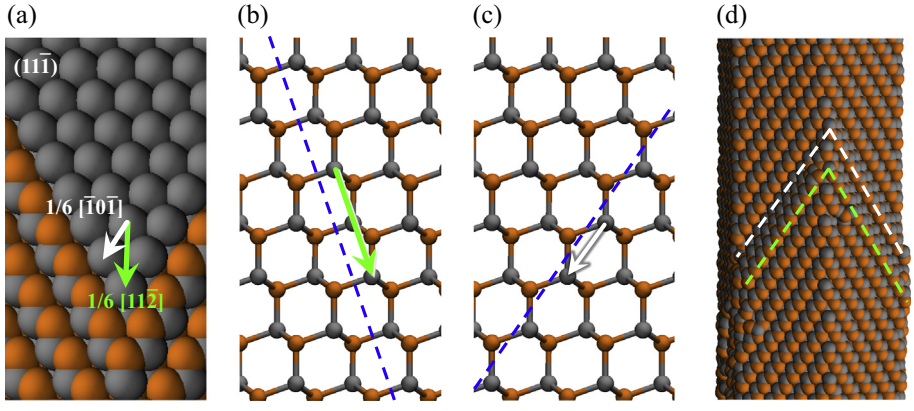

Fig. 3. Details of dislocation activities in GaAs NRs. (a) Two partial dislocations with Burgers vectors of $1/6[\bar{1}\ 0\ \bar{1}]$ and $1/6[1\ 1\ \bar{2}]$ on the $(1\ 1\ \bar{1})$ plane. (b and c) Slip is achieved by breaking and re-bonding the GaAs bonds on intra-close packed planes. Dashed lines indicate the $(1\ 1\ \bar{1})$ planes. (d) A snapshot after two dislocations cut through a sample. White and green lines denote the $(1\ 1\ \bar{1})$ planes after $1/6[\bar{1}\ 0\ \bar{1}]$ and $1/6[11\bar{2}]$ cut through the surface, respectively. (For interpretation of the references to color in this figure legend, the reader is referred to the web version of this article.)

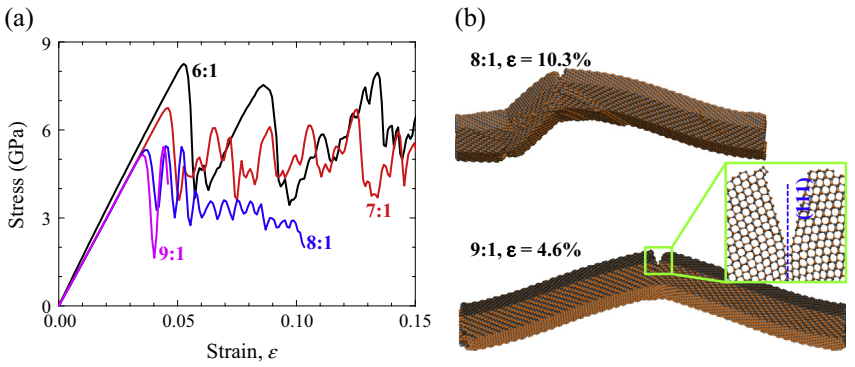

Fig. 4. Length-dependent brittle-to-ductile transition in GaAs NRs. (a) Stress–strain curves of GaAs NRs with a lateral dimension of 5.5 nm and different ARs from 6:1 to 9:1. (b) A NR with an AR = 8:1 eventually subjects to brittle fracture although it undergoes a dislocation dominated plastic deformation. However, brittle fracture of the NR with AR = 9:1 repels any dislocations.

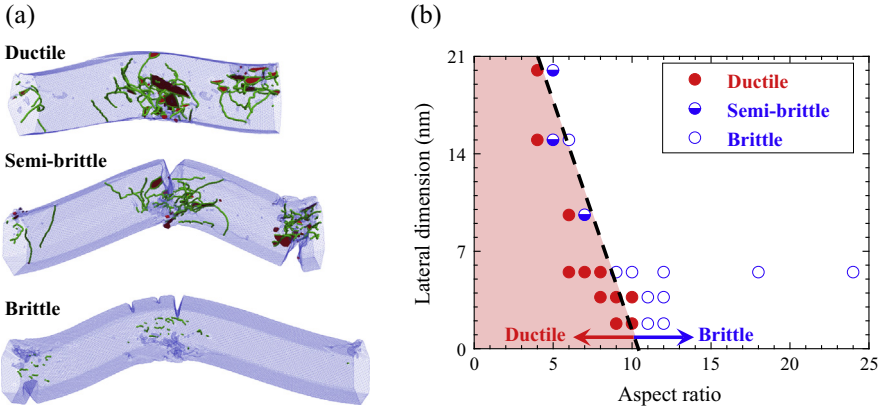

Fig. 5. Size-dependent brittle-to-ductile transition of GaAs NRs. (a) NRs with the same lateral dimension of 15 nm show ductile, semi-brittle and brittle behaviors as their ARs are 4:1, 5:1 and 6:1, respectively. (b) A summary of deformation behaviors of GaAs NRs with various lateral dimensions and ARs. A dashed line implies the critical size to switch the brittle-to-ductile transition.

compressive case, buckling occurs beyond the elastic limit, which results in a non-uniform distribution of stress on a sample. Specifically, one side of a NR bears tensile stress while the opposite side undergoes much severe compression. With further loading, a competition emerges between generation of cracks at the tensile side and initiation of dislocations at the compressive side. The preference to the former leads to brittle fracture. On the contrary, the latter ensures plastic deformation. The competition can be tuned by the critical AR, at which a brittle-to-ductile transition is realized (see Fig. 4). A NR with an AR more than the critical value easily tends to buckling under compression due to its flexibility. This aggravates the stress status at the tensile side and results in the superiority of cracks. With increase of the lateral dimension of a NR, the critical AR reduces since slight bending produces a severe tensile stress at the tensile side. This well explains the brittleness of GaAs at the macro-scale [19,21]. Since tensile brittleness and compressive ductility are also confirmed in ZB SiC NRs [12–14,37], it is expected that there is a similar size-dependent brittle-to-ductile transition.

As shown in Fig. 2c, with the increase of their ARs, the critical buckling strain of GaAs NRs deviates from what is expected by the conventional Euler model. This is mainly due to the positive values of two surface properties: surface elastic modulus and residual surface stress [34]. On the contrary, negative values of these two surface properties may lead to an inverse trend in silicon nanowires [33].

Furthermore, it is worth noting that traces of the $1/6[\bar{1}\ 0\ \bar{1}]$ and $1/6[1\ 1\ \bar{2}]$ partial dislocations in ZB GaAs differ from those observed in face-centered cubic (FCC) metals. Taking a Ga–As pair (a module of a tetrahedral bonding) as a unit, the ZB structure decays to FCC according to the crystal symmetry. Here a module of a tetrahedral bonding in a ZB GaAs corresponds to a close packed plane in an FCC metal. Since slip in GaAs occurs at intra-close packed planes, the original ABC sacking sequence remains unchanged. Thus, only a dislocation line is produced after the motion of a partial dislocation in GaAs (see Fig. 6), which can be evidenced by means of a central symmetry parameter [38]. In an FCC metal, however, slip is along inter-close packed planes. That is, the motion of a partial dislocation alters the original stacking sequence of an FCC metal and thus a stacking fault is generated (see Fig. 6). This is why partial dislocation-generated stacking faults are widely observed in FCC metals and alloys [39–41].

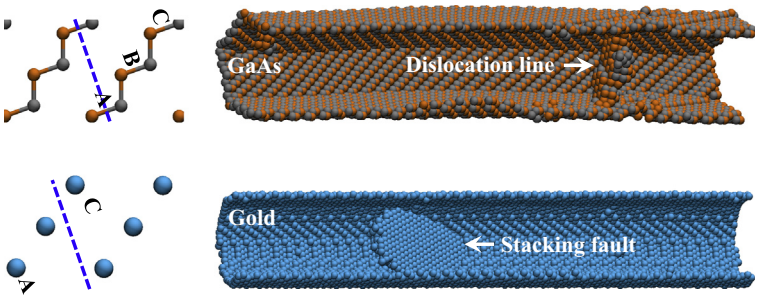

Fig. 6. Propagation of $1/6[1\ 1\ \bar{2}]$ dislocation in GaAs only generates a dislocation line, while it leads to formation of a stacking fault in gold. A, B and C denote close packed stacking sites. Dashed lines are slip planes.

5. Conclusion

In summary, experimentally observed compressive ductility of GaAs NRs has been investigated by using MD simulations. A significant size-dependent brittle-to-ductile transition is demonstrated due to the competition between generation of cracks and initiation of dislocations. Such a competition is regulated by a critical aspect ratio of NRs, below which dislocation activities dominate plastic deformation and otherwise the preference to cracks yields brittle fracture. The critical aspect ratio reduces with the increase of lateral dimensions of NRs. This finding provides a recipe for the design of semiconductors with ductility at room temperature.

Acknowledgements

This work has been supported by the National Natural Science Foundation of China (Grant Nos. 11172024, 11232013 and 11372022), the National Basic Research Program of China (2012CB937500), the Scientific Research Foundation for the Returned Overseas Chinese Scholars, State Education Ministry, the Opening Fund of State Key Laboratory of Nonlinear Mechanics (LNM), the Research Grant Council of the Hong Kong Special Administrative Region, China [Project No. 9041679 (CityU 120611)], and the Australian Research Council (Grant No. DP0985450). Computations were performed on the ScGrid of Supercomputing Center, Computer Network Information Center of Chinese Academy of Sciences, the LNMGrid of the State Key Laboratory of Nonlinear Mechanics and the Pawsey Supercomputing Centre with funding from the Australian Government and the Government of Western Australia.

References

[1] Yoon J, Jo S, Chun IS, Jung I, Kim H-S, Meitl M, et al. GaAs photovoltaics and optoelectronics using releasable multilayer epitaxial assemblies. Nature 2010;465:329–33.
[2] Qin Y, Wang XD, Wang ZL. Microfiber-nanowire hybrid structure for energy scavenging. Nature 2008;451:809–13.
[3] Wang XD, Song JH, Liu J, Wang ZL. Direct current nanogenerator driven by ultrasonic wave. Science 2007;316(5821):102–5.
[4] Mélinon P, Masenelli B, Tournus F, Perez A. Playing with carbon and silicon at the nanoscale. Nat Mater 2007;6:479–90.
[5] Mishnaevsky Jr L, Dai GM. Hybrid and hierarchical nanoreinforced polymer composites: computational modelling of structure–properties relationships. Compos Struct 2014;117:156–68.
[6] Wu JY, He JY, Odegard GM, Nagao S, Zheng QS, Zhang ZL. Giant stretchability and reversibility of tightly wound helical carbon nanotubes. J Am Chem Soc 2013;135(37):13775–85.
[7] Raihanuzzaman RM, Xie ZH, Hong SJ, Ghomashchi R. Powder refinement, consolidation and mechanical properties of cemented carbides – an overview. Powder Technol 2014;261:1–13.
[8] Agrawal R, Espinosa HD. Giant piezoelectric size effects in zinc oxide and gallium nitride nanowires: a first principles investigation. Nano Lett 2011;11(2):786–90.
[9] Chen CQ, Shi Y, Zhang YS, Zhu J, Yan YJ. Size dependence of young's modulus in ZnO nanowires. Phys Rev Lett 2006;96(7):075505.
[10] Kulkarni AJ, Zhou M, Ke FJ. Orientation and size dependence of the elastic properties of zinc oxide nanobelts. Nanotechnology 2005;16(12):2749–56.
[11] Agrawal R, Peng B, Gdoutos EE, Espinosa HD. Elasticity size effects in ZnO nanowires – a combined experimental-computational approach. Nano Lett 2008;8(11):3668–74.
[12] Han XD, Zhang YF, Zheng K, Zhang XN, Zhang Z, Hao YJ, et al. Low-temperature in situ large strain plasticity of ceramic SiC nanowires and its atomic-scale mechanism. Nano Lett 2007;7(2):452–7.
[13] Zhang YF, Han XD, Zheng K, Zhang Z, Zhang XN, Fu J, et al. Direct observation of super-plasticity of beta-SiC nanowires at low temperature. Adv Funct Mater 2007;17(17):3435–40.
[14] Wang J, Lu C, Wang Q, Xiao P, Ke FJ, Bai YL, et al. Understanding large plastic deformation of SiC nanowires at room temperature. Europhys Lett 2011;95(6):63003.
[15] Kan S, Mokari T, Rothenberg E, Banin U. Synthesis and size-dependent properties of zinc-blende semiconductor quantum rods. Nat Mater 2003;2:155–8.
[16] Huang XY, Makmal A, Chelikowsky JR, Kronik L. Size-dependent spintronic properties of dilute magnetic semiconductor nanocrystals. Phys Rev Lett 2005;94(23):236801.
[17] Wang Y, Herron N. Nanometer-sized semiconductor clusters: materials synthesis, quantum size effects, and photophysical properties. J Phys Chem 1991;95(2):525–32.
[18] Joyce HJ, Gao Q, Tan HH, Jagadish C, Kim Y, Zhang X, et al. Twin-free uniform epitaxial GaAs nanowires grown by a two-temperature process. Nano Lett 2007;7(4):921–6.

[19] Wang YB, Joyce HJ, Gao Q, Liao XZ, Tan HH, Zou J, et al. Self-healing of fractured GaAs nanowires. Nano Lett 2011;11(4):1546–9.
[20] Wang J, Lu C, Wang Q, Xiao P, Ke FJ, Bai YL, et al. Self-healing of fractured one-dimensional brittle nanostructures. Europhys Lett 2012;98(1):16010.
[21] Wang YB, Wang LF, Joyce HJ, Gao Q, Liao XZ, Mai Y-W, et al. Super deformability and Young's modulus of GaAs nanowires. Adv Mater 2011;23(11):1356–60.
[22] Chen B, Wang J, Gao Q, Chen YJ, Liao XZ, Lu C, et al. Strengthening brittle semiconductor nanowires through stacking faults: insights from in situ mechanical testing. Nano Lett 2013;13(9):4369–73.
[23] Shan ZW, Mishra RK, Asif SAS, Warren OL, Minor AM. Mechanical annealing and source-limited deformation in submicrometre-diameter Ni crystals. Nat Mater 2007;432(2):115–9.
[24] Heo YW, Norton DP, Tien LC, Kwon Y, Kang BS, Ren F, et al. ZnO nanowire growth and devices. Mater Sci Engng R 2004;47(1–2):1–47.
[25] Sköld N, Wagner JB, Karlsson G, Hernan T, Seifert W, Pistol M, et al. Phase segregation in AlInP shells on GaAs nanowires. Nano Lett 2006;6(12):2743–7.
[26] Humphrey W, Dalke A, Schulten K. VMD: visual molecular dynamics. J Mol Graphics 1996;14(1):33–8.
[27] Su X, Kalia RK, Nakano A, Vashishta P, Madhukar A. InAs/GaAs square nanomesas: multimillion-atom molecular dynamics simulations on parallel computers. J Appl Phys 2003;94(10):6762–73.
[28] Melchionna S, Ciccotti G, Holian BL. Hoover NPT dynamics for systems varying in shape and size. Mol Phys 1993;78(3):533–44.
[29] Smith W, Yong CW, Rodger PM. DL_POLY: application to molecular simulation. Mol Simul 2002;28(5):385–471.
[30] Nosé S. A molecular dynamics method for simulations in the canonical ensemble. Mol Phys 1984;52(2):255–68.
[31] Hoover WG. Canonical dynamics: equilibrium phase-space distributions. Phys Rev A 1985;31(3):1695–7.
[32] Wang J, Soh AK, Xiao P, Ke FJ. Molecular-dynamics investigation on polarization retention of barium titanate nanofilm arising from ordered oxygen vacancy. Europhys Lett 2010;92(1):17006.
[33] Park HS. Surface stress effects on the critical buckling strains of silicon nanowires. Comput Mater Sci 2012;51(1):396–401.
[34] Wang GF, Feng XQ. Surface effects on buckling of nanowires under uniaxial compression. Appl Phys Lett 2009;94(14):141913.
[35] Wang J, Lu C, Wang Q, Xiao P, Ke FJ, Bai YL, et al. Self-healing in fractured GaAs nanowires. Acta Mater 2012;60(15):5593–600.
[36] Stukowski A, Albe K. Extracting dislocations and non-dislocation crystal defects from atomistic simulation data. Modell Simul Mater Sci Engng 2010;18(8):085001.
[37] Wang J, Lu C, Wang Q, Xiao P, Ke FJ, Bai YL, et al. Influence of microstructures on mechanical behaviours of SiC nanowires: a molecular dynamics study. Nanotechnology 2012;23(2):025703.
[38] Kelchner CL, Plimpton SJ, Hamilton JC. Dislocation nucleation and defect structure during surface indentation. Phys Rev B 1998;58(17):11085.
[39] Zhan HF, Gu YT, Yan C, Feng XQ, Yarlagadda PKDV. Numerical exploration of plastic deformation mechanisms of copper nanowires with surface defects. Comput Mater Sci 2011;50(12):3425–30.
[40] Yu WS, Shen SP. Initial dislocation topologies of nanoindentation into copper (001) film with a nanocavity. Engng Fract Mech 2010;77(16):3329–40.
[41] Baker KL, Warner DH. An atomistic investigation into the nature of near threshold fatigue crack growth in aluminum alloys. Engng Fract Mech 2014;115:111–21.